https://doi.org/10.5194/egusphere-2024-550
Preprint. Discussion started: 11 March 2024

Widespread increase of root zone storage capacity in the United States

Jiaxing Liang[1], Hongkai Gao[1]*, Fabrizio Fenicia[2], Qiaojuan Xi[1], Yahui Wang[1], Hubert H. G. Savenije[3]

[1] School of Geographic Sciences, East China Normal University, Shanghai, China

[2] Eawag, Swiss Federal Institute of Aquatic Science and Technology, Dubendorf, Switzerland

[3] Water Resources Section, Delft University of Technology, Delft, the Netherlands

*Corresponding author. Email: hkgao@geo.ecnu.edu.cn

https://orcid.org/0000-0003-0786-8067

Abstract

The root zone is the upper part of the unsaturated zone, where water and nutrients are accessible to plants, controlling hydrological responses, vegetation dynamics, biogeochemical processes, and land-atmospheric interaction. The root zone storage capacity (S_{umax}) represents the maximum subsurface moisture volume that can be accessed by the vegetation's roots, controlling the partitioning of precipitation into storage, runoff and percolation. Previous work has illustrated that S_{umax} varies spatially, largely responding to climatic conditions. It can be therefore expected that S_{umax} varies temporally as well in response to climate change. However, this hypothesis has not been tested. In this study, we utilized a conceptual hydrological model and a dynamic parameter identification analysis method, to quantify the temporal trends of S_{umax} for 497 catchments in the USA. We found that 423 catchments (85%) showed increasing S_{umax}, which averagely increased from 178 to 235 mm between 1980 and 2014. The increasing trend was also validated by multi-sources data and independent methods. Our results suggest that ecosystems dynamically adapt their root zone in response to climate change, which significantly affects hydrological processes and water resources availability. Moreover, the increase of S_{umax} significantly correlates to hydroclimatic indicators and vegetation dynamics. These results highlight the importance of considering the co-evolution of climate, ecosystems, and hydrology.

https://doi.org/10.5194/egusphere-2024-550
Preprint. Discussion started: 11 March 2024

1. Introduction

The root zone water storage capacity (S_{umax}) is the size of a conceptualized bucket in the unsaturated zone of the soil in which vegetation buffers water during wet periods to sustain transpiration during dry periods (Gao et al., 2014a). The real shape of the S_{umax} is hard to determine, as it consists of a complex of pores and fissures in the substrate and extends both laterally and in depth. Generally, this volume is normalized by the area, and it is therefore represented as a depth. The S_{umax} forms a crucial link between ecosystems and hydrological processes (Dralle et al., 2018; de Boer-Euser et al., 2019a; Gao et al., 2023). It controls the partitioning of precipitation in flow generation and plant use. It forms a core parameter in conceptual hydrological models (Fenicia et al., 2011; Seibert and Vis, 2012; Zhao, 1992; Gao et al., 2023). The accurate estimation of S_{umax} is essential for global and regional hydrological simulation, land surface processes, and dynamic vegetation modeling.

Observing S_{umax} directly is impractical. Traditional methods use field measurements of rooting depth and soil texture to estimate plot scale S_{umax}, under the assumption that soil properties determine plant available moisture (Jackson et al., 1996; Schenk and Jackson, 2002). However, this method is labor intensive, costly and destructive. Moreover, it only provides local and sparse estimates with large uncertainty of upscaling. More importantly, this method provides instantaneous measurements, which cannot reflect the dynamic response of the root zone to climate change or human activities.

An inverse approach to determine S_{umax} is to look at ecosystem performance and what it does to buffer against dry spells. The water-balance based Mass Curve Technique (MCT) provides a powerful tool to derive the root zone storage capacity by observable land surface moisture fluxes, including precipitation, snowmelt, evaporation, runoff, and human-induced irrigation (Gao et al., 2014a; Wang-Erlandsson et al., 2016). Another inverse approach to determine S_{umax} is by parameter calibration (Fenicia et al., 2008a; Gharari et al., 2014; Merz et al., 2011), which can serve as a benchmark in well-gauged catchment-scale studies. This method also has uncertainties, mostly associated to model parameter equifinality and the difficulty of relating model parameters to catchment characteristics. However, such problems can be attenuated through specific modelling choices, and this method can provide useful indications of otherwise unobservable properties.

It is well documented that, because of climate change and land-use management, ecosystems have adjusted their above-ground biomass, leading to a greening trend at global-scale (Lele and Krishnaswamy, 2019; Chen et al., 2019). However, little is known about terrestrial ecosystems' root zone adaption to these changes. To explore the root zone dynamics, we used multi-source datasets to determine temporal changes of S_{umax} and compared them to other environmental indicators.

In this study, we utilized a large-scale catchment dataset of 497 catchments in the USA. We used two independent approaches for S_{umax} estimation. The first

https://doi.org/10.5194/egusphere-2024-550
Preprint. Discussion started: 11 March 2024

one uses a parsimonious conceptual hydrological model (FLEX), which is calibrated in a moving time window, using the Dynamic Identification Analysis method (DYNIA) approach (Wagener et al., 2003). The second approach is based on the MCT method, with the ERA-5 reanalysis grid-cell data as forcing, which provides the root zone storage capacity in different ecosystems required to overcome certain return periods of droughts, i.e. 5, 10, 20, 30, 40 years. We compared the values and trends of root zone storage capacities from these two independent methods and analyzed the temporal trends of S_{umax} in relation to environmental variables.

2. Data and Methods

2.1 Data

The hydrometeorological data used in this study is the CAMELS (Catchment Attributes and MEteorology for Large-sample Studies) dataset (https://doi.org/10.5065/D6MW2F4D) (Addor et al., 2017). The CAMELS dataset comprises daily meteorological data and catchment attributes from 1980 to 2014 for 671 catchments across the United States. It covers a wide variety of hydroclimatic conditions, including long streamflow time series from catchments with limited impact by human activities. Catchment-scale precipitation and temperature were obtained from the Daymet data set (Thornton et al., 2012). Potential evaporation was estimated based on temperature data, using the Hargreaves equation (Hargreaves et al., 1985). The NDVI data is the current release of the NOAA Global Inventory Monitoring and Modeling System (GIMMS) long series (1981-2015) homogenized vegetation index product with version number 3g.v1 (https://doi.org/10.3334/ORNLDAAC/2187) (NCAR, 2018; Pinzon and Tucker, 2014; Thornton et al., 2016).

The catchments with missing daily data were eliminated, and only those with complete data were retained. This filtering resulted into 497 catchments (Figure 1). The 497 catchments were classified into 10 clusters according to Jehn et al. (2020), based on climate, hydrology and location. The 10 clusters are determined using a principal component analysis based on Ward's linkage method (Ward, 1963). Figure 1 and Table 1 present distribution maps and detailed information for 10 clusters, while Figure 2 illustrates the temporal trends of hydroclimatic variables and NDVI for these 10 clusters.

ERA5 reanalysis precipitation, evaporation, snowmelt and irrigation data are also used as part of the methodology in order to provide an independent validation (https://cds.climate.copernicus.eu/cdsapp#!/software/app-c3s-daily-era5-statistics?tab=app). In particular, this data will be used as input for the MCT method (see Section 2.4), to estimate the temporal variation of root zone storage capacity.

https://doi.org/10.5194/egusphere-2024-550
Preprint. Discussion started: 11 March 2024

2.2 Model calibration approach

2.2.1 Model description

The first approach for estimating S_{umax} is based on model calibration. The model used in this research is based on the FLEX hydrological model (Fenicia et al., 2009; Fenicia et al., 2011; Gao et al., 2014b). The model is composed of reservoirs, lag functions and junction elements to represent different hydrological functions constructed with the flexible modelling framework SUPERFLEX (Fenicia et al., 2011). It includes five reservoirs (Figure 1): a snow reservoir (S_w), an interception reservoir (S_i), a root zone reservoir (S_u), a fast-response reservoir (S_f) and a slow-response reservoir (S_s). The water budget equation and structural equation of different reservoirs are shown in Table 2. There are 10 free parameters that need to be calibrated, as shown in Table 3, which describes the role of each parameter and the bound of its value.

Precipitation is stored in snowpack or interception reservoirs before entering the root zone reservoir. Snow accumulation and melting are calculated based on a degree day factor algorithm. When the temperature is below the threshold temperature T_t (°C), precipitation P (mm day^{-1}) occurs as snowfall (P_s, mm day^{-1}), and increases the storage in snow reservoirs S_w. When the temperature is above the threshold temperature T_t, the amount of snow melting M can be calculated from the parameter F_{DD} (mm d^{-1} ℃$^{-1}$) (Eq. (7)).

The precipitation retained in the interception reservoirs is directly returned to the atmosphere by evaporation. The interception evaporation E_i (mm d^{-1}) is the same as potential evaporation E_p (mm day^{-1}) if there is water in the reservoir. The storage volume in the interception reservoir is S_i and the maximum storage capacity is I_{max} (mm) (Eqs. (8) to (10)).

The core of this hydrological model is the root zone module, which determines the partitioning of effective precipitation (P_e) into either runoff generation (R_u) or evaporation (E_a).

The actual evaporation E_a (mm d^{-1}) in the soil is determined by potential evaporation E_p, actual storage in root zone S_u, S_{umax} (mm) and parameter C_e (-) (Eq. (12)). Runoff generation (R_u) is determined by the amount of effective precipitation (P_e), the actual storage in root zone (S_u), and the root zone moisture storage capacity (S_{umax}). In equations (13) and (14), C_r (-) represents the runoff coefficient, β (-) is the spatial diversity factor, and R_u (mm) represents the generated flow during rainfall events, obtained by multiplying the effective rainfall and snowmelt P_e (mm) entering the soil module by the runoff coefficient C_r.

The generated runoff R_u is divided through the parameter D (-) into fast response runoff and slow response runoff (Eq. (15) and Eq. (16)). Equations (17) and (18) were used to describe the time lag between storm and fast runoff. R_f (mm) is the generated fast runoff, T_{lag} (d) is a parameter which represents the lag-time between storm and fast runoff generation, *c(i)* is the weight of the flow in *i-1* days before and R_{fl} (mm) is the runoff into the fast-response reservoir S_f after convolution. Slow runoff R_s (mm) into the slow-response reservoir S_s.

https://doi.org/10.5194/egusphere-2024-550
Preprint. Discussion started: 11 March 2024

A linear equation was used to conceptualize the flows in the fast response reservoirs and slow response reservoirs. In equations (20) and (22), S_f and S_s represent the fast and the slow reservoirs; K_f (d) and K_s (d) represent the fast and slow receding coefficient; Q_f and Q_s represent the fast and slow runoff, respectively, while simulated runoff Q_m is the sum of the Q_f and Q_s.

2.2.2 Dynamic parameter identification and model evaluation

The assessment of the temporal variation of parameters is based on the Dynamic Identification Analysis method (DYNIA) proposed by Wagener et al. (2003). DYNIA is based on a Monte Carlo framework and employs a Latin hypercube sampling technique. In this study, we generated 40,000 sets of parameter combinations within the feasible range for the 10 parameters. Each set of parameters is associated to a streamflow simulation, for which a performance metric is calculated. In this study, the Kling-Gupta efficiency (KGE) proposed by Gupta et al. (2009) and modified by Kling et al. (2012) was used to calculate the model simulation performance. Model performance was calculated using a five-year moving window, using the first year of each period as a warm-up. For each period and each catchment, the optimal model (with highest KGE) was selected. Subsequently, we considered the 10 catchments clusters provided by Jehn et al. (2020), and averaged the optimal parameters for all catchments in the same cluster and period. The simulation results of temporal trends for all 10 parameters of 10 clusters are shown in Figure 4.

2.3 MCT method

As an alternative to model calibration, root zone storage capacity has been determined through the mass balance method using merely climatic data. This storage capacity is referred to as S_R, which is subsequently compared to the model-derived S_{umax} as an independent validation.

The MCT method estimates S_R based on the principle of the water balance (Gao et al., 2014a; Wang-Erlandsson et al., 2016). When the outflow (F_{out}) from the root zone (i.e. evaporation) exceeds the inflow (F_{in}) (i.e. infiltration), then the water deficit is calculated by computing the difference between the two. This water deficit requires plants to draw water from storage (S_R). Vegetation's canopy interception (I) is also considered in the MCT method, to make corresponding comparison with the calibrated FLEX.

F_{in} represents the sum of net precipitation (P-I), snowmelt (SM), and irrigation (IRR):

$$F_{\mathrm{in}} = P - I + SM + IRR \quad (18)$$

Since E in ERA-5 data is the total evaporation, including canopy interception, the evaporation from root zone (F_{out}) must subtract the amount of interception from the total evaporation:

$$F_{\mathrm{out}} = E - I \quad (19)$$

The difference between outflow and inflow then equals $P + SM + IRR - E$, where the interception drops out. This difference is accumulated on a daily scale:

https://doi.org/10.5194/egusphere-2024-550
Preprint. Discussion started: 11 March 2024

$$A(t_n \rightarrow t_{n+1}) = \int_{t_n}^{t_{n+1}} F_{out} - F_{in} dt \quad (20)$$

Where $A(t_n \rightarrow t_{n+1})$ represents the water deficit on day t_{n+1}. The sum of daily water deficits constitutes the cumulative water demand:

$$D_e(t_{n+1}) = \max(0, D_e(t_n) + A(t_n \rightarrow t_{n+1}))(21)$$

$D_e(t_{n+1})$ represents the cumulative water deficit on day t_{n+1}. The accumulation of D_e only occurs during periods when $F_{out} > F_{in}$, while a reduction in D_e occurs when $F_{out} < F_{in}$. Additionally, D_e has a minimum value of 0. The required root zone storage capacity S_R represents the maximum value of D_e:

$$S_R = \max(D_e(t_0), D_e(t_1), D_e(t_2), \ldots, D_e(t_{end}),)(22)$$

To account for the impacts of multi-year droughts, we allow the deficit D_e accumulation continues in the end of the end, and extends into the following year. Then the maximum D_e of that year is regarded as the year's S_R. Since S_{umax} is simulated using a five-year time window, to make fair comparison, the maximum S_R value over the same five-year period was compared with S_{umax}.

Different ecosystems have different strategies to cope with drought. For instance, forests, due to their longer lifetime, have a strong drought adaptation requirement, resulting in a root zone storage capacity to overcome a drought that may occur once in 20-40 years, while shrubs, having a shorter lifetime, exhibit weaker adaptation demands, lasting through droughts occurring less frequently than once every 20 years. Grasslands, on the other hand, can go dormant and may accept a much higher probability of drought. Seasonal crops may permit a probability of failure of once in 5 years. As a result, we calculated S_R for different drought return periods (S_{R10y}, S_{R20y} and S_{R40y}) by applying the Gumbel distribution to the yearly S_R (Gumbel, 1935). Many studies have shown that the MCT method for estimating S_R is reliable (de Boer-Euser et al., 2016, 2019b; Sakschewski et al., 2021; Wang et al., 2021; Wang-Erlandsson et al., 2016). The MCT method utilizes the ERA-5 dataset, introduced in Section 2.1.

2.4 Correlation analysis

The Spearman correlation coefficient was utilized to quantify the correspondence between temporal trends of S_{umax} and catchment environmental changes. For each catchment, we calculated the time series correlation between the catchment's precipitation P, runoff Q, temperature T, potential evaporation Ep, runoff coefficient Q/P, evaporation coefficient E/P=1-Q/P (assuming the delta of water storage at annual scale is small), aridity index AI, precipitation seasonality index SI, $NDVI$ and S_{umax}. Each indicator is representative of a 5 years period, with 7 data points in each regression. Results are shown in section 3.3.

https://doi.org/10.5194/egusphere-2024-550
Preprint. Discussion started: 11 March 2024

3.Results

3.1. Climate and environment changes

First we analyzed the changes in climate and vegetation data for the 497 study catchments from 1980 to 2014. We adopted the clusters provided by Jehn et al. (2020) to classify 497 catchments into 10 clusters, according to catchments characteristics in terms of climate, hydrology and location. These 10 clusters capture the unique hydrologic behavior of the continental United States and represent catchment groups with distinctly different hydrologic behavior. Figure 2 shows the spatially mean variations of precipitation *P*, runoff *Q*, temperature *T*, potential evaporation *Ep*, and *NDVI* for the catchments in 10 clusters.

The average annual precipitation of clusters 3, 5, 6, and 7 generally exceed 1500 mm/yr, and clusters 1, 4, and 7 are the second largest with above 1000 mm/yr. Clusters 2, 8, and 9 are drier, with the lowest precipitation (<1000 mm/yr). The runoff characteristics of the catchments also reflect this precipitation pattern. From 1980 to 2014, all clusters experienced an upward trend in mean temperature, with cluster 3 showing the most significant increase of nearly 2°C. There were interannual variations in potential evaporation in 10 clusters, but no clear trends were observed. Except for clusters 3, the mean NDVI of the remaining clusters displayed an upward trend. There was a noticeable abrupt change occurring around 1990. Specifically, the most significant increase in NDVI took place before and after this time.

3.2. Spatial Patterns of S_{umax} and S_R

We compared the S_{umax} parameter of the FLEX model (representing the root zone storage capacity in catchment scale by parameter calibration) with the S_R obtained from the MCT method (representing the root zone storage capacity in grid scale by land surface fluxes measurements, modeling and data assimilation), both exhibit similar spatial patterns in terms of magnitude and range (Figure 3).

Consistently with the predefined clusters, we found that catchments in the same cluster tend to behave similarly and catchments in different cluster can have different behavior. In particular, within clusters 1, 3, and 9, S_{umax} exhibits the highest consistency with the 10-year drought return period (S_{R10y}) results. Clusters 4 and 7 are most aligned with S_{R20y}. Conversely, clusters 2, 5, 6, 8 and 10 are closest to S_{R40y}. The average root zone storage capacity for all catchments in the CAMELS dataset is most in line with the results for a 20-year drought return period (S_{R20y}).

Clusters 2 and 8 represent arid catchments with larger S_{umax} values (>200mm), where vegetation often possesses deeper root systems to meet their water needs and avoid water stress. Cluster 9 is highly similar to Cluster 8 in terms of catchment characteristics but features higher forest coverage, with the

https://doi.org/10.5194/egusphere-2024-550
Preprint. Discussion started: 11 March 2024

widest range in S_{umax} distribution (200-300mm). The S_{umax} values in Clusters 5, 6, and 7 are approximately 200mm. These catchments share similar characteristics (Jehn et al., 2020) and are all located in the West Coast forest region (Figure 1), known for abundant precipitation and strong seasonality. Cluster 6 exhibits the most pronounced seasonality among all clusters, with the majority of precipitation occurring in winter. By the end of summer, catchments in this cluster are nearly completely dry. On the contrary, catchments in Clusters 3, 4, and 10, characterized by higher relative humidity and vegetation cover, exhibit lower S_{umax} values.

3.3. Temporal variation of S_{umax} and S_R

The temporal variations of 10 the parameters of the FLEX model, calculated using the DYNIA method, are shown in Figure 4. Except for the trend of S_{umax}, there are some other interesting trends. For example, the threshold temperature, T_t, controlling the split of snowfall and rainfall, dramatically increased in the catchments of cluster 3, which have large amount snowpack. We believe it is worthwhile to conduct further studies to understand the impacts of climate change on this essential snow-related parameter. However, since this is out the scope of this study, we did not implement detailed research, and focused this study on the temporal change of S_{umax}。

The DYNIA results reveal that from 1980 to 2014, the annual average S_{umax} for all 497 catchments increased from 178 mm to 235 mm, marking a 32% increase, with a linear regression rate of 1.91 mm/yr (Figure 5). Across the 10 clusters, all S_{umax} values exhibited an overall increasing trend. Specifically, Clusters 1, 2, 9, and 10 showed noticeable upward trends, with Cluster 9 demonstrating the most significant increase, having a linear slope of 2.73 mm/yr. In contrast, Cluster 3 displayed the smallest growth in S_{umax}, with a slope of only 0.03 mm/yr. Cluster 3 is characterized by a relatively small number of catchments, only 6 in total, and is notable for its abundant snowfall (Jehn et al., 2020). As shown in Figure 4, snow processes may play a more significant role than the root zone in influencing S_{umax}. The increase of S_{umax} suggests that the ecosystems in these catchments adapted to environmental change by increasing their root zone storage capacity (Dai, 2011; Gamelin et al., 2022).

The S_R values obtained from the MCT method are highly comparable to S_{umax}. The annual average S_{R20y} for all 497 catchments also exhibited an increasing trend, rising from 190 to 222 mm, with a linear regression rate of 1.07 mm/yr. From 1980 to 2014, S_R increased by 32 mm, which is considerably less than the increase in S_{umax} derived from calibration. Among the 10 clusters, 8 clusters displayed an increasing trend in S_R, consistent with the trend in S_{umax}. The only exceptions were Clusters 6 and 7, which showed decreasing trends with S_{R40y} and S_{R20y} slopes of -0.74 mm/yr and -0.19 mm/yr, respectively. We will discuss the possible reasons in the discussion.

Furthermore, from the perspective of individual catchments, S_{umax} increased in 85 % (423) of the catchments and decreased in 15 % (74) of the catchments (Figure 6a). Catchments with increase in S_{umax} were distributed throughout the United States, while catchments with decrease in S_{umax} were concentrated in the

https://doi.org/10.5194/egusphere-2024-550
Preprint. Discussion started: 11 March 2024

western and central regions of the United States. This indicates that the widespread increase of S_{umax} occurs in most catchments in the United States.

Figure 6b demonstrated the comparison of the trends of S_{R} and S_{umax} in 497 catchments. Among these, 400 catchments exhibit an increasing trend in S_{R}, while 97 catchments show a decreasing trend. In two-thirds (69%) of the catchments, both S_{umax} and S_{R} display consistent increasing trends. Additionally, 17 catchments (3%) exhibit consistent decreasing trends in both S_{umax} and S_{R}. 28% of the catchments demonstrated opposing trends between S_{umax} and S_{R}. Overall, root zone storage capacity (S_{umax} and S_{R}) obtained using different methods and different data exhibit similar trends and magnitudes in most catchments (72%). The comparable results obtained by multi-sources datasets and independent methods suggest that the trend changes in S_{umax} do represent the significant ecohydrological changes, rather than the result of parameter uncertainties resulting from model calibration.

3.4. Relationship between environmental change and S_{umax} variation

When comparing the variability of S_{umax} with other indicators, it can be seen that the temporal variation of S_{umax} exhibits a positive correlation with P, T, Ep, E/P, SI and $NDVI$ in most catchments (Figure 7). The median correlation coefficients range from 0.07 to 0.46. On the contrary, the temporal variation of S_{umax} is negatively correlated with Q, Q/P and AI, and median range from -0.21 to -0.46. The temporal variation of S_{umax} shows the strongest positive correlation with E/P (evaporation coefficient) and consequently the strongest negative correlation with Q/P (runoff coefficient), which in the long term equals 1-E/P. The significant correlation of S_{umax} with hydroclimatic indicators underscores the interdependency of vegetation and hydrology, emphasizing the importance of studying changes in root zone storage capacity for understanding hydrological responses under changing conditions.

The correlations between environmental factors and S_{umax} can vary significantly among different clusters or catchments, even when the same combination of factors is present (Figure 8). This variability can be interpreted as arising from differences in catchment topography and hydrological processes. For example, the results of our research demonstrate that S_{umax} and AI show a negative temporal correlation in most catchments. Theoretically, the availability of vegetation water is influenced by the humidity of the catchment, with larger S_{umax} observed in regions of higher aridity (Stocker et al., 2023). However, the trend of S_{umax} was negatively correlated with the AI in most of the catchments in the clusters (1, 3, 5, 6, 7, 10) in wetter regions (Figure. 8g). This may be explained by the fact that in wet regions, where vegetation is less constrained by water availability, changes in S_{umax} are primarily influenced by other environmental factors than AI (Green et al., 2022). With climate becoming wetter (Figure 2), i.e. when the drought index decreases, root zone storage capacity may increase due to other factors such as rising temperature and nutrient availability, which would lead to an increase in $NDVI$, and consequently, greater vegetation water demand, resulting in an increase in S_{umax}. This ultimately creates a negative correlation between S_{umax} and AI.

https://doi.org/10.5194/egusphere-2024-550
Preprint. Discussion started: 11 March 2024

Cluster 4, although located in a humid region, receives relatively low precipitation, primarily due to low *AI* caused by cooler temperatures in mountainous areas (Figure 2). Climate warming not only increased *AI* but also enhanced vegetation productivity, jointly driving an increase in root zone water demand. Hence, Cluster 4 tends to show a positive correlation. Only a few arid cluster catchments (2, 8, 9) are primarily dominated by the *AI*, leading to a positive correlation in most of the catchments.

4. Discussions

The comparison of the two independent approaches for estimating root zone storage, as shown in Figure 3 shows a consistent behavior between the ERA-5 derived S_R and S_{umax}. This result suggests that both approaches identify the same variable, which we associate to the root zone storage capacity. There are similar parameters determining the splitter of runoff generation and infiltration to meet water deficit (and eventually used for evaporation during dry spells) in hydrological models, such as the tension water capacity in the Xinanjiang model (Zhao et al., 1992; Hu et al., 2004), the maximum soil water storage (or field capacity in original version) in the HBV hydrological model (Lindström et al., 1997; Seibert et al., 2022), and the maximum capacity of the production store in the GR4J model (Perrin et al., 2003). Among these models, Xinanjiang model used a probability distribution curve to represent the catchment characteristic of storage capacity, thus with more solid physical foundation (Moore, 2007). That is the reason we chose the Xinanjiang curve as root zone storage capacity distribution in this study.

Long-term catchment-scale streamflow and spot-scale lysimeter measurements revealed that root zone seepage matched perfectly with catchment runoff in the Rietholzbach research catchment in Switzerland, although these two observations have large scale discrepancy (see Figure 4 in Seneviratne et al., 2012). Moreover, Nijzink et al. (2016) compared S_R derived from water balance with the S_{umax} parameters of four hydrological models, revealing remarkably similar patterns in the three studied catchments in the United States. All these experimental and modeling studies using multi-source data and independent methods further confirmed that S_{umax} does represent the root zone storage capacity.

For the trend of S_{umax}, we found that, over the years, S_{umax} is increasing in the United States and that this increase can be largely attributed to climate change. This corresponds to the results of Merz et al. (2011), who used the HBV model to simulate 273 catchments in Austria and found that the soil water storage parameter FC nearly doubled from 150 to 275 mm in 30 years and attributed it to increases in temperature and evaporation.

As a survival strategy, plants adopt a cost minimization in the design of their root systems, aiming to meet the water demands of the canopy with the minimum allocation of root carbon (Milly, 1994). In the Mediterranean climate region with strong seasonality of precipitation, abundant rainfall during the wet season boosts vegetation productivity, leading to a deeper rooting system (Fan et al., 2017). During the dry season, vegetation may rely on tap roots to access groundwater (Dawson and Pate, 1996). In forest areas with sufficient water supply, rainfall thoroughly saturates the soil, and due to frequent surface wetting, the root systems do not require access to deep water. The spatial distribution of S_{umax} observed in this study is consistent with the results of Gao et al. (2014a), who calculated the root zone storage capacity for over 300 catchments using Model Parameter Estimation Experiment (MOPEX) data. Both studies demonstrated the increase of S_{umax} in response to an increase of the aridity index, i.e. geospatially from the humid east coast to the dry inland regions of the United States. Additionally, this study extends the analysis of S_{umax} from spatial to temporal variability under changing environmental conditions.

This study compared the root zone storage capacity calculated by two different methods and datasets (S_{umax} and S_{R}). Disparities were observed between the two outcomes, such as significant differences in the magnitude of trend slopes between S_{umax} and S_{R}. These disparities may be attributed to the presence of croplands in certain catchments, which are heavily influenced by human activities. The MCT method accounted for these human activities, such as irrigation and artificial reservoirs, which increase water supply to the root zone during dry seasons, thereby alleviating water shortage and leading to S_{R} reduction compared to natural ecosystems. On the other hand, the discrepancy may have resulted from scale mismatches, i.e. the S_{umax} at catchment scale and the S_{R} derived from ERA5 data (spatial resolution of 0.5 degree) used by the MCT method. It is difficult to draw solid conclusion on which method is more reliable than the other. From the perspective of methodology, both methods have a strong physical basis. But the MCT method explicitly considers the human activities, such as irrigation, on atmospheric moisture fluxes; while they have implicit impact on DYNIA results through the runoff, although it is difficult to isolate the influence of human activities. From the perspective of forcing data uncertainty, MCT method in this study is based on the ERA-5 land surface reanalysis data; while DYNIA method is based on observed hydrological data, which is normally more reliable in a catchment scale study. There may be other reasons causing the different magnitudes. We still need more studies to understand this issue and close the gap between two independent methods.

This study employed two methods to calculate root zone storage capacity, both methodologies calculated the total evaporation without differentiating between transpiration from vegetation and soil evaporation. Thus, this is a fair comparison. Moreover, soil evaporation constitutes a relatively small proportion of the terrestrial hydrological fluxes, around 6% of the total evaporation in a global scale analysis (see Good et al., 2015). This proportion is even lower in regions with vegetation cover, which is the predominant land cover in most catchments of this study. Hence, vegetation water use transpiration from root zone is an overwhelmingly major flux dominating dry spell evaporation.

Our results show a positive correlation of S_{umax} with E/P and a negative correlation with Q/P (which in the long term equals 1- E/P) According to the Budyko framework (Marlatt et al., 1975; Donohue et al., 2006) (the relation between aridity Ep/P and E/P), the division of flow into runoff and evaporation

https://doi.org/10.5194/egusphere-2024-550
Preprint. Discussion started: 11 March 2024

is highly influenced by S_{umax} (Cheng et al., 2017; Gentine et al., 2012; Luo et al., 2020; Gerrits, 2009). An increase in S_{umax} implies increased plant transpiration, leading to higher E/P and lower Q/P. As a result, catchments with decreased S_{umax} have higher Q/P and *vice-versa*. By establishing dynamic relationships between model parameters and environmental factors, it challenges the assumption of a static modeling framework. In contrast, allowing dynamic model parameters would allow to model the effect of environmental changes on catchment hydrological characteristics.

5. Conclusions

In this study, we used a large sample dataset to estimate the temporal variation of S_{umax} through dynamic parameter identification of the FLEX hydrological model. The aim was to enhance our understanding of S_{umax} variation in a changing environment and to improve the model's ability to simulate under such conditions. We found that from 1980 to 2014, S_{umax} in most catchments across the United States showed a significant increasing trend. 423 catchments (85%) showed increasing S_{umax}, and the average S_{umax} of the 497 catchments increased from 178 to 235 mm, representing a 32% increase.

The S_R obtained through the MCT method exhibited similar spatial distribution and temporal patterns to S_{umax}, not only affirming the authenticity of S_{umax} growth without calibration-induced artifacts but also emphasizing that the hydrological model parameter S_{umax} indeed represents root zone storage capacity. This indicates that the constantly changing climate significantly changes the ecohydrological processes of the catchment, compelling vegetation to adjust its root zone storage capacity to adapt to the environment.

Furthermore, the temporal correlation analysis between S_{umax} and environmental factors reveals a significant negative correlation between S_{umax} and both runoff and runoff coefficient. This indicates a strong connection between ecosystem dynamics and hydrological processes. In summary, using multi-source datasets and independent methods, we found a significant increase of root zone storage capacity in the United States, indicating ecosystems' adaptation of belowground biomass in response to environmental change. It shows that it is important to consider a dynamic root zone in hydrological and land surface modeling studies.

Competing interests

At least one of the (co-)authors is a member of the editorial board of Hydrology and Earth System Sciences.

Acknowledgements

This research has been supported by the National Natural Science Foundation of China (grant no. 42071081 and 42122002).

https://doi.org/10.5194/egusphere-2024-550
Preprint. Discussion started: 11 March 2024

References

Abbass, K., Qasim, M. Z., Song, H., Murshed, M., Mahmood, H., & Younis, I. (2022). A review of the global climate change impacts, adaptation, and sustainable mitigation measures. Environmental Science and Pollution Research, 29(28), 42539–42559. https://doi.org/10.1007/s11356-022-19718-6

Addor, N., Newman, A. J., Mizukami, N., & Clark, M. P. (2017). The CAMELS data set: Catchment attributes and meteorology for large-sample studies. Hydrology and Earth System Sciences, 21(10), 5293–5313. https://doi.org/10.5194/hess-21-5293-2017

Bandh, S. A., Shafi, S., Peerzada, M., Rehman, T., Bashir, S., Wani, S. A., & Dar, R. (2021). Multidimensional analysis of global climate change: A review. Environmental Science and Pollution Research, 28(20), 24872–24888. https://doi.org/10.1007/s11356-021-13139-7

Bevan, S. L., Los, S. O., & North, P. R. J. (2014). Response of vegetation to the 2003 European drought was mitigated by height. Biogeosciences, 11(11), 2897–2908. https://doi.org/10.5194/bg-11-2897-2014

Beven, K., & Binley, A. (1992). The future of distributed models: Model calibration and uncertainty prediction. Hydrological Processes, 6(3), 279–298. https://doi.org/10.1002/hyp.3360060305

Brigode, P., Oudin, L., & Perrin, C. (2013). Hydrological model parameter instability: A source of additional uncertainty in estimating the hydrological impacts of climate change? Journal of Hydrology, 476, 410–425. https://doi.org/10.1016/j.jhydrol.2012.11.012

Brunner, I., Herzog, C., Dawes, M. A., Arend, M., & Sperisen, C. (2015). How tree roots respond to drought. Frontiers in Plant Science, 6. https://doi.org/10.3389/fpls.2015.00547

Chen, C., Park, T., Wang, X., Piao, S., Xu, B., Chaturvedi, R. K., Fuchs, R., Brovkin, V., Ciais, P., Fensholt, R., Tømmervik, H., Bala, G., Zhu, Z., Nemani, R. R., & Myneni, R. B. (2019). China and India lead in greening of the world through land-use management. Nature Sustainability, 2(2), 122–129. https://doi.org/10.1038/s41893-019-0220-7

Cheng, L., Zhang, L., Chiew, F. H. S., Canadell, J. G., Zhao, F., Wang, Y., Hu, X., & Lin, K. (2017). Quantifying the impacts of vegetation changes on catchment storage-discharge dynamics using paired-catchment data. Water Resources Research, 53(7), 5963–5979. https://doi.org/10.1002/2017WR020600

Dai, A. (2011). Drought under global warming: A review. WIREs Climate Change, 2(1), 45–65. https://doi.org/10.1002/wcc.81

Dawson, T. E., & Pate, J. S. (1996). Seasonal water uptake and movement in root systems

https://doi.org/10.5194/egusphere-2024-550
Preprint. Discussion started: 11 March 2024

of Australian phraeatophytic plants of dimorphic root morphology: A stable isotope investigation. Oecologia, 107(1), 13–20. https://doi.org/10.1007/BF00582230

de Boer-Euser, T., McMillan, H. K., Hrachowitz, M., Winsemius, H. C., & Savenije, H. H. G. (2016). Influence of soil and climate on root zone storage capacity. Water Resources Research, 52(3), 2009–2024. https://doi.org/10.1002/2015WR018115

de Boer-Euser, T., Meriö, L., & Marttila, H. (2019a). Understanding variability in root zone storage capacity in boreal regions. Hydrology and Earth System Sciences. doi:10.5194/HESS-23-125-2019

de Boer-Euser, T., Palalane, J., Savenije, H., & Juízo, D. (2019b). How climate variations are reflected in root zone storage capacities. Physics and Chemistry of the Earth, Parts A/B/C, 112, 83–90. https://doi.org/10.1016/j.pce.2019.04.006

Deng, C., Liu, P., Wang, D., & Wang, W. (2018). Temporal variation and scaling of parameters for a monthly hydrologic model. Journal of Hydrology, 558, 290–300. https://doi.org/10.1016/j.jhydrol.2018.01.049

Donohue, R.J., Roderick, M.L., & McVicar, T.R. (2006). On the importance of including vegetation dynamics in Budyko's hydrological model. Hydrology and Earth System Sciences, 11, 983-995. doi:10.5194/HESS-11-983-2007

Dralle, D. N., Hahm, W. J., Rempe, D. M., Karst, N. J., Thompson, S. E., & Dietrich, W. E. (2018). Quantification of the seasonal hillslope water storage that does not drive streamflow. Hydrological Processes, 32(13), 1978–1992. https://doi.org/10.1002/hyp.11627

Fan, Y., Miguez-Macho, G., Jobbágy, E. G., Jackson, R. B., & Otero-Casal, C. (2017). Hydrologic regulation of plant rooting depth. Proceedings of the National Academy of Sciences, 114(40), 10572–10577. https://doi.org/10.1073/pnas.1712381114

Feddes, R. A., Hoff, H., Bruen, M., Dawson, T., De Rosnay, P., Dirmeyer, P., Jackson, R. B., Kabat, P., Kleidon, A., Lilly, A., & Pitman, A. J. (2001). Modeling Root Water Uptake in Hydrological and Climate Models. Bulletin of the American Meteorological Society, 82(12), 2797–2809. https://doi.org/10.1175/1520-0477(2001)082<2797:MRWUIH>2.3.CO;2

Feng, H., & Zhang, M. (2015). Global land moisture trends: Drier in dry and wetter in wet over land. Scientific Reports, 5(1), 18018. https://doi.org/10.1038/srep18018

Fenicia, F., Kavetski, D., & Savenije, H. H. G. (2011). Elements of a flexible approach for conceptual hydrological modeling: 1. Motivation and theoretical development. Water Resources Research, 47(11), 2010WR010174. https://doi.org/10.1029/2010WR010174

Fenicia, F., McDonnell, J. J., & Savenije, H. H. G. (2008). Learning from model improvement: On the contribution of complementary data to process understanding. Water Resources Research, 44(6), 2007WR006386. https://doi.org/10.1029/2007WR006386

Fenicia, F., Savenije, H. H. G., & Avdeeva, Y. (2009). Anomaly in the rainfall-runoff

https://doi.org/10.5194/egusphere-2024-550
Preprint. Discussion started: 11 March 2024

behaviour of the Meuse catchment. Climate, land-use, or land-use management? Hydrology and Earth System Sciences, 13(9), 1727–1737. https://doi.org/10.5194/hess-13-1727-2009

Gao, H., Fenicia, F., & Savenije, H. H. G. (2023). HESS Opinions: Are soils overrated in hydrology? Hydrology and Earth System Sciences, 27(14), 2607–2620. https://doi.org/10.5194/hess-27-2607-2023

Gao, H., Hrachowitz, M., Fenicia, F., Gharari, S., & Savenije, H. H. G. (2014b). Testing the realism of a topography-driven model (FLEX-Topo) in the nested catchments of the Upper Heihe, China. Hydrology and Earth System Sciences, 18(5), 1895–1915. https://doi.org/10.5194/hess-18-1895-2014

Gao, H., Hrachowitz, M., Schymanski, S. J., Fenicia, F., Sriwongsitanon, N., & Savenije, H. H. G. (2014a). Climate controls how ecosystems size the root zone storage capacity at catchment scale. Geophysical Research Letters, 41(22), 7916–7923. https://doi.org/10.1002/2014GL061668

Gamelin, B. L., Feinstein, J., Wang, J., Bessac, J., Yan, E., & Kotamarthi, V. R. (2022). Projected U.S. drought extremes through the twenty-first century with vapor pressure deficit. Scientific Reports, 12(1), 8615. https://doi.org/10.1038/s41598-022-12516-7

Gentine, P., D'Odorico, P., Lintner, B. R., Sivandran, G., & Salvucci, G. (2012). Interdependence of climate, soil, and vegetation as constrained by the Budyko curve. Geophysical Research Letters, 39(19), 2012GL053492. https://doi.org/10.1029/2012GL053492

Gerrits, A. M. J., Savenije, H. H. G., Veling, E. J. M., & Pfister, L. (2009). Analytical derivation of the Budyko curve based on rainfall characteristics and a simple evaporation model. Water Resources Research, 45(4), 2008WR007308. https://doi.org/10.1029/2008WR007308

Gharari, S., Hrachowitz, M., Fenicia, F., Gao, H., & Savenije, H. H. G. (2014). Using expert knowledge to increase realism in environmental system models can dramatically reduce the need for calibration. Hydrology and Earth System Sciences, 18(12), 4839–4859. https://doi.org/10.5194/hess-18-4839-2014

Good, S. P., Noone, D., & Bowen, G. (2015). Hydrologic connectivity constrains partitioning of global terrestrial water fluxes. Science, 349(6244), 175–177. https://doi.org/10.1126/science.aaa5931

Green, J. K., Ballantyne, A., Abramoff, R., Gentine, P., Makowski, D., & Ciais, P. (2022). Surface temperatures reveal the patterns of vegetation water stress and their environmental drivers across the tropical Americas. Global Change Biology, 28(9), 2940–2955. https://doi.org/10.1111/gcb.16139

Gupta, H. V., Kling, H., Yilmaz, K. K., & Martinez, G. F. (2009). Decomposition of the mean squared error and NSE performance criteria: Implications for improving hydrological modelling. Journal of Hydrology, 377(1–2), 80–91.

https://doi.org/10.1016/j.jhydrol.2009.08.003

Hahm, W. J., Dralle, D. N., Rempe, D. M., Bryk, A. B., Thompson, S. E., Dawson, T. E., & Dietrich, W. E. (2019). Low Subsurface Water Storage Capacity Relative to Annual Rainfall Decouples Mediterranean Plant Productivity and Water Use From Rainfall Variability. Geophysical Research Letters, 46(12), 6544–6553. https://doi.org/10.1029/2019GL083294

Hargreaves, G. L., Hargreaves, G. H., & Riley, J. P. (1985). Agricultural Benefits for Senegal River Basin. Journal of Irrigation and Drainage Engineering, 111(2), 113–124. https://doi.org/10.1061/(ASCE)0733-9437(1985)111:2(113)

Hu, C., Guo, S., Xiong, L., & Peng, D. (2005). A modified Xinanjiang model and its application in northern China. Hydrology Research, 36(2), 175–192. https://doi.org/10.2166/nh.2005.0013

Jehn, F. U., Bestian, K., Breuer, L., Kraft, P., & Houska, T. (2020). Using hydrological and climatic catchment clusters to explore drivers of catchment behavior. Hydrology and Earth System Sciences, 24(3), 1081–1100. https://doi.org/10.5194/hess-24-1081-2020

Kling, H., Fuchs, M., & Paulin, M. (2012). Runoff conditions in the upper Danube basin under an ensemble of climate change scenarios. Journal of Hydrology, 424–425, 264–277. https://doi.org/10.1016/j.jhydrol.2012.01.011

Larson, D. W. (2001). The paradox of great longevity in a short-lived tree species. Experimental Gerontology, 36(4–6), 651–673. https://doi.org/10.1016/S0531-5565(00)00233-3

Lee, J.-E., Oliveira, R. S., Dawson, T. E., & Fung, I. (2005). Root functioning modifies seasonal climate. Proceedings of the National Academy of Sciences, 102(49), 17576–17581. https://doi.org/10.1073/pnas.0508785102

Lele, S., & Krishnaswamy, J. (2019). Climate Change and India's Forests. in N. K. Dubash (Edit), India in a Warming World (1, 477–497). Oxford University PressDelhi. https://doi.org/10.1093/oso/9780199498734.003.0026

Lindström, G., Johansson, B., Persson, M., Gardelin, M., & Bergström, S. (1997). Development and test of the distributed HBV-96 hydrological model. Journal of Hydrology, 201(1–4), 272–288. https://doi.org/10.1016/S0022-1694(97)00041-3

Luo, Y., Yang, Y., Yang, D., & Zhang, S. (2020). Quantifying the impact of vegetation changes on global terrestrial runoff using the Budyko framework. Journal of Hydrology, 590, 125389. https://doi.org/10.1016/j.jhydrol.2020.125389

Marlatt, W. E., Budyko, M. I., & Miller, D. H. (1975). Climate and Life. Journal of Range Management, 28(2), 160. https://doi.org/10.2307/3897455

Merz, R., Parajka, J., & Blöschl, G. (2011). Time stability of catchment model parameters: Implications for climate impact analyses. Water Resources Research, 47(2), 2010WR009505. https://doi.org/10.1029/2010WR009505

Milly, P. C. D. (1994). Climate, soil water storage, and the average annual water balance.

https://doi.org/10.5194/egusphere-2024-550
Preprint. Discussion started: 11 March 2024

Water Resources Research, 30(7), 2143–2156. https://doi.org/10.1029/94WR00586

Montanari, A. (2005). Large sample behaviors of the generalized likelihood uncertainty estimation (GLUE) in assessing the uncertainty of rainfall-runoff simulations. Water Resources Research, 41(8), 2004WR003826. https://doi.org/10.1029/2004WR003826

Nijzink, R., Hutton, C., Pechlivanidis, I., Capell, R., Arheimer, B., Freer, J., Han, D., Wagener, T., McGuire, K., Savenije, H., & Hrachowitz, M. (2016). The evolution of root-zone moisture capacities after deforestation: A step towards hydrological predictions under change? Hydrology and Earth System Sciences, 20(12), 4775–4799. https://doi.org/10.5194/hess-20-4775-2016

Perrin, C., Michel, C., & Andréassian, V. (2003). Improvement of a parsimonious model for streamflow simulation. Journal of Hydrology, 279(1–4), 275–289. https://doi.org/10.1016/S0022-1694(03)00225-7

Pinzon, J., & Tucker, C. (2014). A Non-Stationary 1981–2012 AVHRR NDVI3g Time Series. Remote Sensing, 6(8), 6929–6960. https://doi.org/10.3390/rs6086929

Ponce-Campos, G. E., Moran, M. S., Huete, A., Zhang, Y., Bresloff, C., Huxman, T. E., Eamus, D., Bosch, D. D., Buda, A. R., Gunter, S. A., Scalley, T. H., Kitchen, S. G., McClaran, M. P., McNab, W. H., Montoya, D. S., Morgan, J. A., Peters, D. P. C., Sadler, E. J., Seyfried, M. S., & Starks, P. J. (2013). Ecosystem resilience despite large-scale altered hydroclimatic conditions. Nature, 494(7437), 349–352. https://doi.org/10.1038/nature11836

Prieto, I., Armas, C., & Pugnaire, F. I. (2012). Water release through plant roots: New insights into its consequences at the plant and ecosystem level. New Phytologist, 193(4), 830–841. https://doi.org/10.1111/j.1469-8137.2011.04039.x

Savenije, H. H. G. (2010). HESS Opinions "Topography driven conceptual modelling (FLEX-Topo)" Hydrology and Earth System Sciences, 14(12), 2681–2692. https://doi.org/10.5194/hess-14-2681-2010

Savenije, H. H. G., & Hrachowitz, M. (2017). HESS Opinions Catchments as meta-organisms – a new blueprint for hydrological modelling. Hydrology and Earth System Sciences, 21(2), 1107–1116. https://doi.org/10.5194/hess-21-1107-2017

Seibert, J., & Vis, M. J. P. (2012). Teaching hydrological modeling with a user-friendly catchment-runoff-model software package. Hydrology and Earth System Sciences, 16(9), 3315–3325. https://doi.org/10.5194/hess-16-3315-2012

Seibert, J., & Bergström, S. (2022). A retrospective on hydrological catchment modelling based on half a century with the HBV model. Hydrology and Earth System Sciences, 26(5), 1371–1388. https://doi.org/10.5194/hess-26-1371-2022

Seneviratne, S. I., Lehner, I., Gurtz, J., Teuling, A. J., Lang, H., Moser, U., Grebner, D., Menzel, L., Schroff, K., Vitvar, T., & Zappa, M. (2012). Swiss prealpine Rietholzbach research catchment and lysimeter: 32 year time series and 2003 drought event. Water Resources Research, 48(6), 2011WR011749.

https://doi.org/10.5194/egusphere-2024-550
Preprint. Discussion started: 11 March 2024

https://doi.org/10.1029/2011WR011749

Singh, C., Wang-Erlandsson, L., Fetzer, I., Rockström, J., & Van Der Ent, R. (2020). Rootzone storage capacity reveals drought coping strategies along rainforest-savanna transitions. Environmental Research Letters, 15(12), 124021. https://doi.org/10.1088/1748-9326/abc377

Stocker, B. D., Tumber-Dávila, S. J., Konings, A. G., Anderson, M. C., Hain, C., & Jackson, R. B. (2023). Global patterns of water storage in the rooting zones of vegetation. Nature Geoscience, 16(3), 250–256. https://doi.org/10.1038/s41561-023-01125-2

Thornton, P. E., Thornton, M. M., Mayer, B. W., Wei, Y., Devarakonda, R., Vose, R. S., & Cook, R. B. (2016). Daymet: Daily Surface Weather Data on a 1-km Grid for North America, Version 3. ORNL Distributed Active Archive Center. https://doi.org/10.3334/ORNLDAAC/1328

Wagener, T., McIntyre, N., Lees, M. J., Wheater, H. S., & Gupta, H. V. (2003). Towards reduced uncertainty in conceptual rainfall-runoff modelling: Dynamic identifiability analysis. Hydrological Processes, 17(2), 455–476. https://doi.org/10.1002/hyp.1135

Wallner, M., & Haberlandt, U. (2015). Non-stationary hydrological model parameters: A framework based on SOM-B: NON-STATIONARY HYDROLOGICAL MODEL PARAMETERS BASED ON SOM-B. Hydrological Processes, 29(14), 3145–3161. https://doi.org/10.1002/hyp.10430

Wang-Erlandsson, L., Bastiaanssen, W. G. M., Gao, H., Jägermeyr, J., Senay, G. B., van Dijk, A. I. J. M., Guerschman, J. P., Keys, P. W., Gordon, L. J., & Savenije, H. H. G. (2016). Global root zone storage capacity from satellite-based evaporation. Hydrology and Earth System Sciences, 20(4), 1459–1481. https://doi.org/10.5194/hess-20-1459-2016

Wang, J., Gao, H., Liu, M., Ding, Y., Wang, Y., Zhao, F., & Xia, J. (2021). Parameter regionalization of the FLEX-Global hydrological model. Science China Earth Sciences, 64(4), 571–588. https://doi.org/10.1007/s11430-020-9706-3

Ward, J. H. (1963). Hierarchical Grouping to Optimize an Objective Function. Journal of the American Statistical Association, 58(301), 236–244. https://doi.org/10.1080/01621459.1963.10500845

Zeng, X., Dai, Y., Dickinson, R. E., & Shaikh, M. (1998). The role of root distribution for climate simulation over land. Geophysical Research Letters, 25(24), 4533–4536. https://doi.org/10.1029/1998GL900216

Zhang, W., Li, Y., Wu, X., Chen, Y., Chen, A., Schwalm, C. R., & Kimball, J. S. (2021). Divergent Response of Vegetation Growth to Soil Water Availability in Dry and Wet Periods Over Central Asia. Journal of Geophysical Research: Biogeosciences, 126(6), e2020JG005912. https://doi.org/10.1029/2020JG005912

Zhao, Ren-Jun. (1992). The Xinanjiang model applied in China. Journal of Hydrology, 135(1–4), 371–381. https://doi.org/10.1016/0022-1694(92)90096-E

https://doi.org/10.5194/egusphere-2024-550
Preprint. Discussion started: 11 March 2024

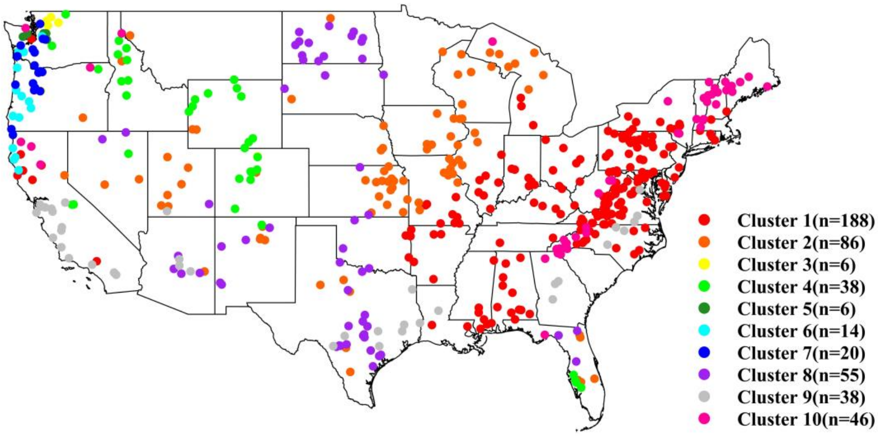

Figure 1 Maps of the 497 CAMELS catchments in the United States, adopted the clusters provided by Jehn et al. (2020).

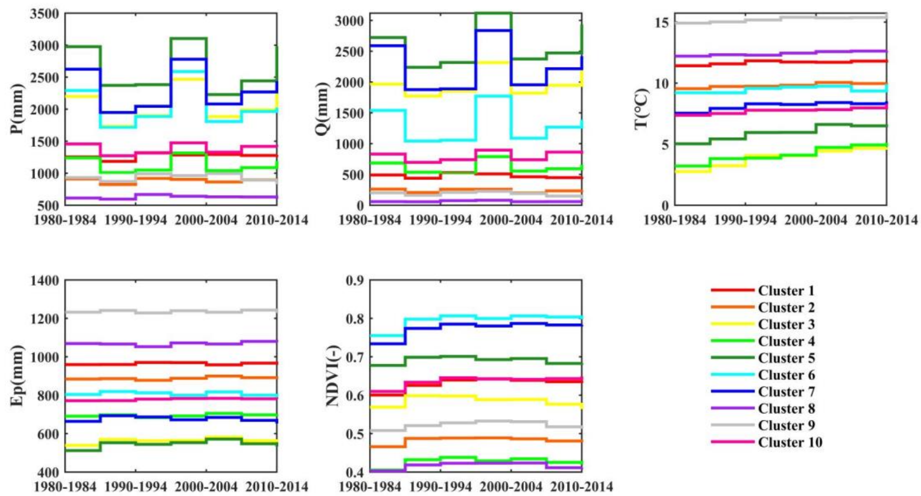

Figure 2 Five-year average temporal trends (mean values) for 10 clusters of precipitation P, runoff Q, temperature T, potential evaporation Ep, and $NDVI$.

https://doi.org/10.5194/egusphere-2024-550
Preprint. Discussion started: 11 March 2024

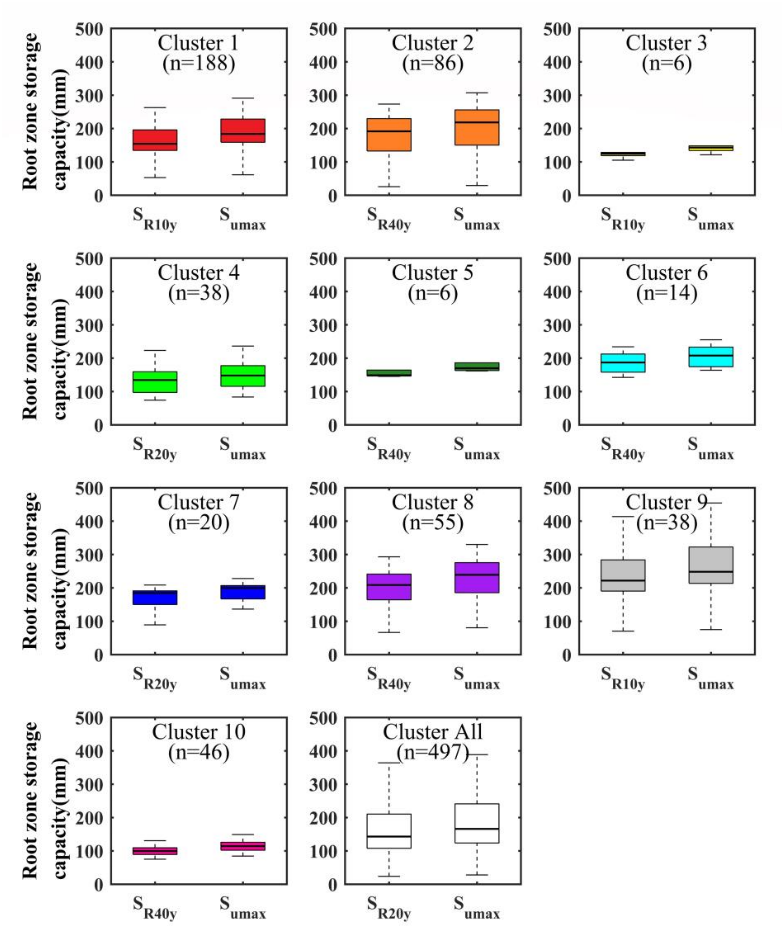

Figure 3 The Box-Whisker plots display the spatial distribution of S_{umax} and S_R (including S_{R10y}, S_{R20y}, and S_{R40y}, representing the required root zone storage capacity to overcome certain return periods of droughts, i.e. 10, 20 and 40 years) across 497 study catchments within 10 clusters. The bottom and top edges of the box representing the 25th and 75th percentiles, respectively. The solid lines represent the median values, while the upper and lower whiskers extend to the furthest data points that are not outliers.

https://doi.org/10.5194/egusphere-2024-550
Preprint. Discussion started: 11 March 2024

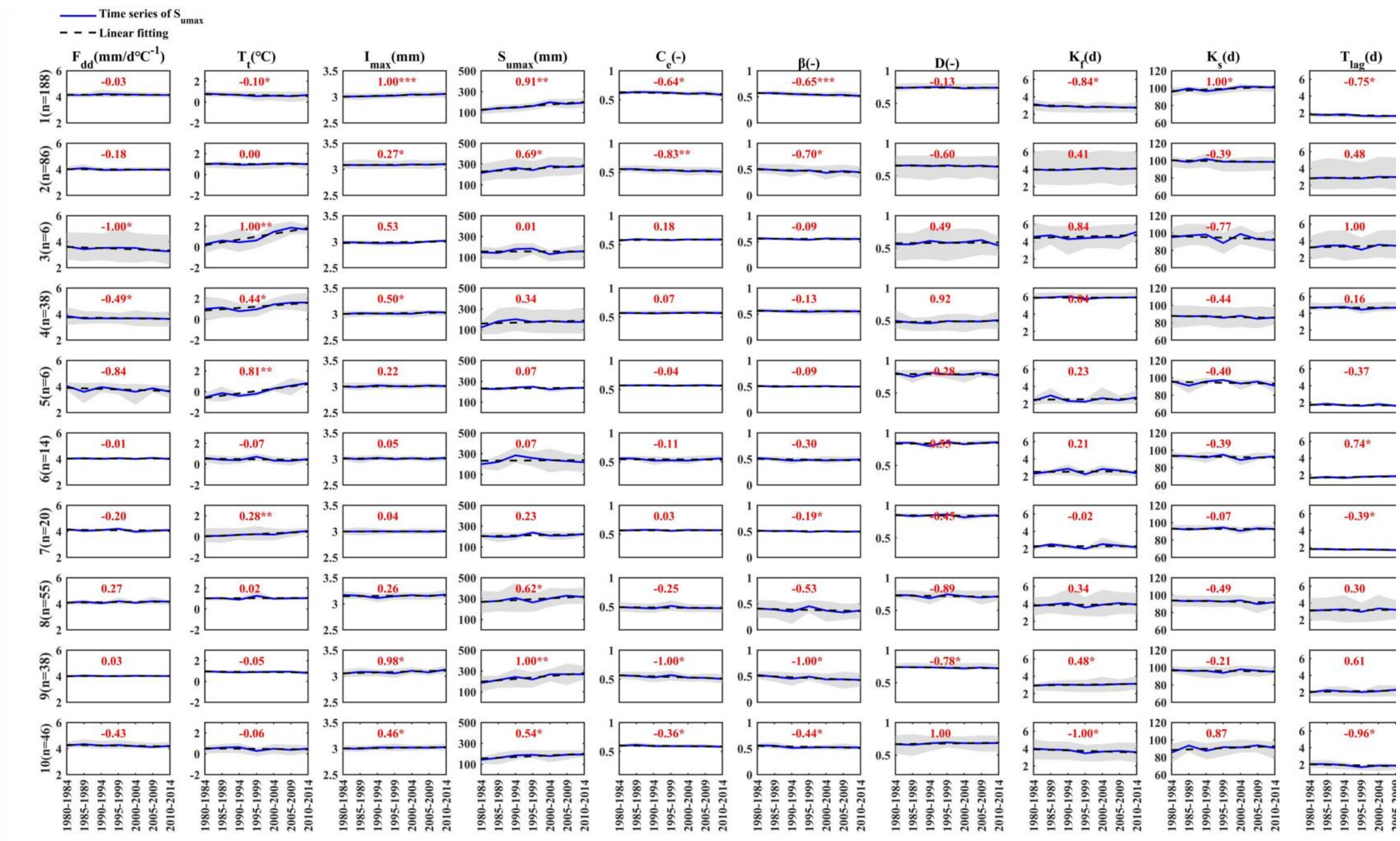

Figure 4 The temporal variations of 10 parameters across 497 study catchments within 10 clusters. The blue solid line represents the average change trend of parameters for all catchments within each cluster. The black dashed line indicates the fitted regression line. The gray shaded area represents the 20%-80% envelop. Standardized regression coefficients are marked in red (above each panel). The significance of regression coefficients is indicated as: '' for 0.1, '' for 0.01, and '' for 0.001.

https://doi.org/10.5194/egusphere-2024-550
Preprint. Discussion started: 11 March 2024

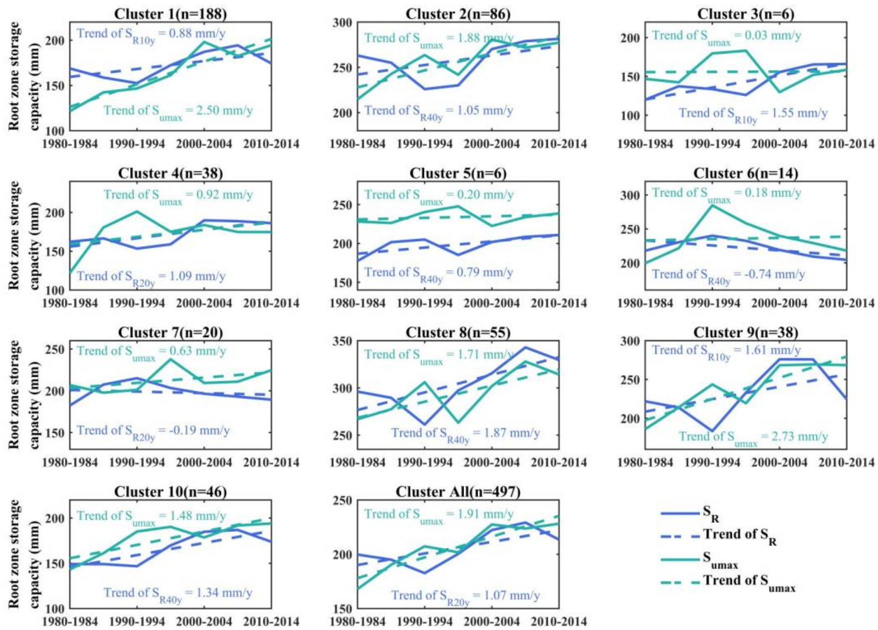

Figure 5 The temporal variations of S_{umax} and S_R (including S_{R10y}, S_{R20y}, and S_{R40y}, representing the required root zone storage capacity to overcome certain return periods of droughts, i.e. 10, 20 and 40 years) across 497 study catchments within 10 clusters. Solid lines represent the average change trend of S_{umax} or S_R for all catchments within each cluster. Dashed lines indicate the fitted regression lines, with corresponding regression coefficients marked in the same color.

https://doi.org/10.5194/egusphere-2024-550
Preprint. Discussion started: 11 March 2024

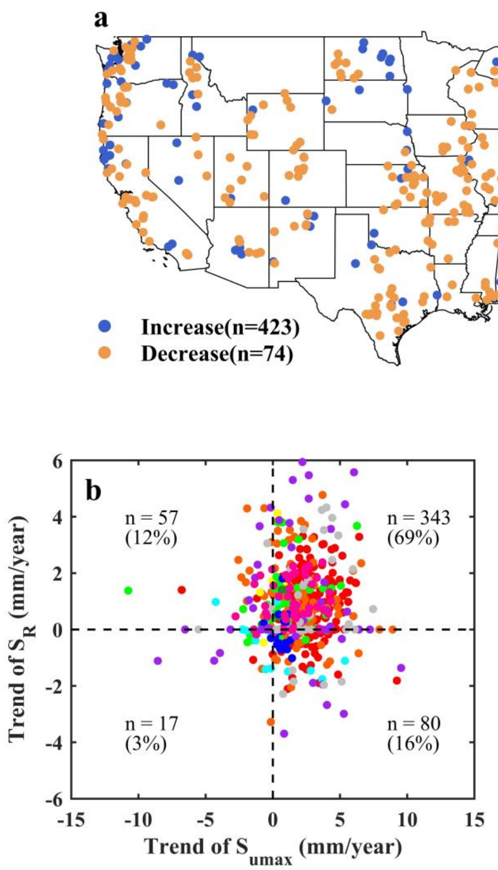

Figure 6 (a) The trend of S_{umax} variation across 497 study catchments: 423 (85%) catchments exhibit an increasing trend, while 74 (15%) catchments show a decreasing trend. (b) The comparative trends of $\mathrm{S}_{\mathrm{umax}}$ and S_{R} across 497 study catchments. Different colored points represent clusters.

https://doi.org/10.5194/egusphere-2024-550
Preprint. Discussion started: 11 March 2024

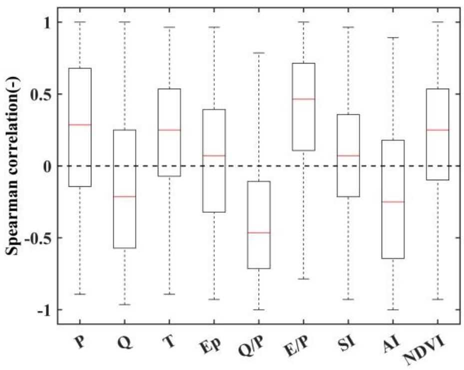

Figure 7 The Box-Whisker plot displays the Spearman temporal correlation coefficients between the S_{umax} model parameters and environmental elements for 497 catchments over a calibration period of seven 5-year cycles. Precipitation *P*, runoff *Q*, temperature *T*, potential evaporation *Ep*, runoff coefficient *Q/P*, evaporation coefficient *E/P*=1-*Q/P* (assuming the delta of water storage at annual scale is small), aridity index *AI*, precipitation seasonality index *SI*. The bottom and top edges of the box representing the 25th and 75th percentiles, respectively. The solid red lines represent the median values, while the upper and lower whiskers extend to the furthest data points that are not outliers.

https://doi.org/10.5194/egusphere-2024-550
Preprint. Discussion started: 11 March 2024

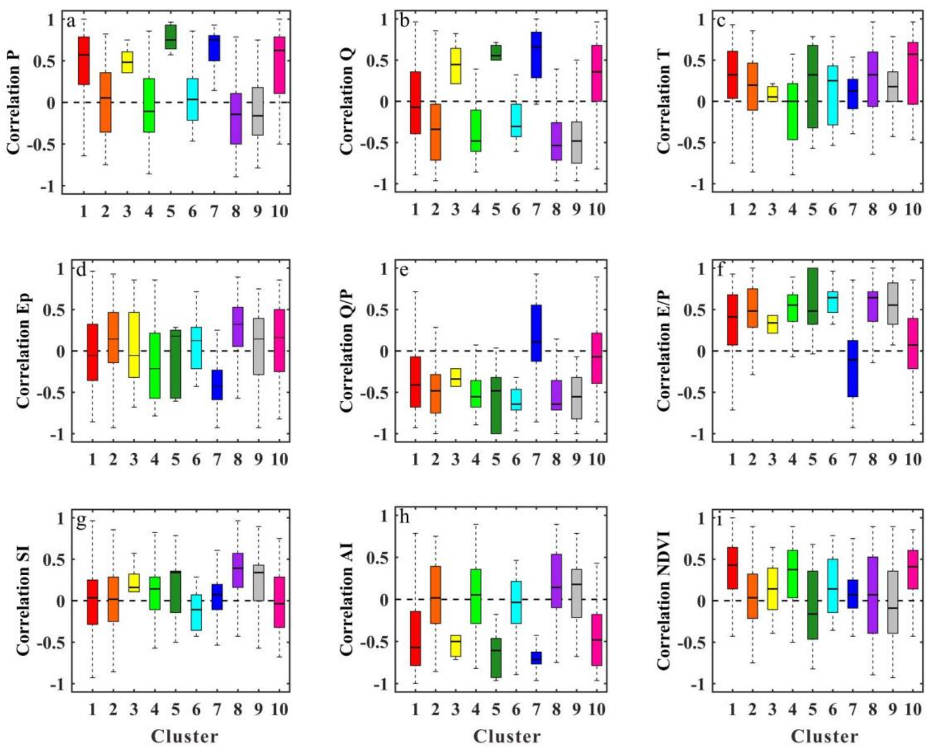

Figure 8 The Box Whisker plot displays the Spearman temporal correlation coefficients between S_{umax} and environmental elements over a calibration period of seven 5-year cycles across 10 clusters of 497 research catchments. The bottom and top edges of the box representing the 25th and 75th percentiles, respectively. The solid lines represent the median values, while the upper and lower whiskers extend to the furthest data points that are not outliers.

https://doi.org/10.5194/egusphere-2024-550
Preprint. Discussion started: 11 March 2024

Table 1 Properties of catchment clusters (Jehn et al., 2020).

Cluster	Number of catchments	Main region	Dominating attribute
1	188	Southeastern and Central Plains	Aridity
2	86	Central Plains (with scattered catchments all over western US)	Green vegetation fraction maximum
3	6	Northwestern Forested Mountains	Fraction of precipitation falling as snow
4	38	Northwestern Forested Mountains and Florida	Precipitation seasonality
5	6	Northern Marine West Coast Forests	Forest fraction
6	14	Marine West Coast Forests	Aridity
7	20	Western Cordillera (Part of Marine West Coast Forests)	Fraction of precipitation falling as snow
8	55	Great Plains and North American deserts	Precipitation seasonality
9	38	All southernmost states of the US	Aridity
10	46	Appalachian Mountains	Mean elevation

https://doi.org/10.5194/egusphere-2024-550
Preprint. Discussion started: 11 March 2024

Table 2 FLEX model water balance equations and structural equations.

Sub-module	Water balance equations	Constructive equations
Snow reservoir	$\frac{dS_{\mathrm{W}}}{dt} = \begin{cases} -M, T > T_{\mathrm{t}} \\ P_{\mathrm{s}}, T \le T_{\mathrm{t}} \end{cases}$ (1)	$M = \begin{cases} \min\left(S_{\mathrm{w}}, F_{\mathrm{DD}}(T - T_{\mathrm{t}})\right), T > T_{\mathrm{t}} \\ 0, T \le T_{\mathrm{t}} \end{cases}$ (2)
Interception reservoir	$\frac{dS_{\mathrm{i}}}{dt} = P_{\mathrm{r}} - E_{\mathrm{i}} - P_{\mathrm{tf}}$(3)	$E_{\mathrm{i}} = \begin{cases} E_{\mathrm{p}}, S_{\mathrm{i}} > 0 \\ 0, S_{\mathrm{i}} = 0 \end{cases}$ (4) $P_{\mathrm{tf}} = \begin{cases} 0, S_{\mathrm{i}} < I_{\mathrm{max}} \\ P_{\mathrm{r}}, S_{\mathrm{i}} = I_{\mathrm{max}} \end{cases}$ (5)
Unsaturated soil reservoir	$\frac{dS_{\mathrm{u}}}{dt} = P_{\mathrm{e}} - E_{\mathrm{a}} - R_{\mathrm{u}}$(6)	$E_a = (E_p - E_i) min(\left(\frac{S_u}{S_{umax} C_e}\right), 1)$(7) $R_{\mathrm{u}} = \begin{cases} P_{\mathrm{e}} - S_{\mathrm{umax}} + S_{\mathrm{u}} + S_{\mathrm{umax}}\left(1 - \frac{P_{\mathrm{e}} + AU}{(1+\beta)S_{\mathrm{umax}}}\right)^{(1+\beta)}; (1+\beta)S_{\mathrm{umax}} > P_{\mathrm{e}} + AU \\ P_{\mathrm{e}} - S_{\mathrm{umax}} + S_{\mathrm{u}}; (1+\beta)S_{\mathrm{umax}} \le P_{\mathrm{e}} + AU \end{cases}$(8) $AU = (1+\beta)S_{\mathrm{umax}}\left(1 - \left(1 - \frac{S_{\mathrm{U}}}{S_{\mathrm{umax}}}\right)^{\left(\frac{1}{1+\beta}\right)}\right)$ (9)

https://doi.org/10.5194/egusphere-2024-550
Preprint. Discussion started: 11 March 2024

Table 2 (Continued).

Splitter and lag function		$R_\mathrm{f} = R_\mathrm{u} D (10); R_s = R_\mathrm{u}(1-D) (11)$ $R_\mathrm{lf} = \sum_{i=1}^{T_\mathrm{lag}} c(i) \cdot R_\mathrm{f}(t-i+1)\ (12)$ $c(i) = i = \sum_{i=1}^{T_\mathrm{lag}} u\ (13)$
Fast reacting reservoir	$\frac{dS_\mathrm{f}}{dt} = R_\mathrm{fl} - Q_\mathrm{f} (14)$	$Q_\mathrm{f} = S_\mathrm{f}/K_\mathrm{f} (15)$
Slow reacting reservoir	$\frac{dS_\mathrm{s}}{dt} = R_\mathrm{s} - Q_\mathrm{s} (16)$	$Q_\mathrm{S} = S_\mathrm{s}/K_\mathrm{s} (17)$

https://doi.org/10.5194/egusphere-2024-550
Preprint. Discussion started: 11 March 2024

Table 3 Description of FLEX model parameters and range of values.

Parameter	Explanation	Range	Units
F_{DD}	Degree day factor	1-7	mm/(d℃$^{-1}$)
T_t	Threshold temperature	-2-4	℃
I_{max}	Maximum S_i storage	1-5	mm
S_{umax}	Root zone storage capacity	30-700	mm
C_e	Threshold of soil moisture content	0.1-1	-
β	Spatial diversity factor	0-1	-
D	Splitter factor	0-1	-
K_f	Fast runoff timescales	1-10	d
K_s	Slow runoff timescales	10-200	d
T_{lag}	Lag-time between storm and fast runoff	0.8-10	d